Internal Temperature Measurements by X-Ray Diffraction on Magnetic Nanoparticles Heated by a High-Frequency Magnetic Field

Stéphane Faure, N Mille, S Kale, J.-M Asensio, J Marbaix, P Farger, D Stoian[2], W van Beek[2], Pier-Francesco Fazzini, Aikaterini Soulantika, et al.

Internal Temperature Measurements by X-Ray Diffraction on Magnetic Nanoparticles Heated by a High-Frequency Magnetic Field

S. Faure*[1], N. Mille*[1], S. Kale[1], J.-M. Asensio[1], J. Marbaix[1], P. Farger[1], D. Stoian[2], W. Van Beek[2], P.-F. Fazzini[1], K. Soulantica[1], B. Chaudret[1], J. Carrey[1]*

[1] Laboratoire de Physique et Chimie des Nano-Objets (LPCNO), Université de Toulouse-INSA-UPS, 135 Avenue de Rangueil, F-31077 Toulouse, France.

[2] Swiss Norwegian Beamlines – ESRF – Grenoble – France

To whom correspondence should be addressed. E-mail: s_faure@insa-toulouse.fr; julian.carrey@insa-toulouse.fr

Abstract: There is a theoretical and experimental controversy on the possibility for magnetic nanoparticles (MNPs) heated by high-frequency magnetic fields to reach a temperature much larger than the one of their environments. Here the internal temperature of magnetically heated magnetite MNPs is measured using the temperature dependence of their lattice parameter, and compared to the one of their environments, measured from reference non-magnetic particles. Within the uncertainty of our experimental methods, which is estimated to be below 5°C, the MNP temperature is the same as the one of their environments.

Keywords: X-rays diffraction; Local temperature; Inductive heating; magnetic nanoparticles; Synthetic natural gas;

1. Introduction

The fact that magnetic nanoparticles (MNPs) generate heat when they are excited by a high-frequency magnetic field permits various potential applications like tumor therapy[1], catalysis[2] or water electrolysis[3]. This diversification has been made possible thanks to continued progresses in the fabrication of chemically-synthesized MNPs, improving the control over their size, shape (core-shell structure, surface morphology), chemical composition and heating power[4]. Magnetic heating allows transferring the energy directly to the MNPs without the need to heat the surrounding (catalysis reactor, human body, electrolyte) and has also the advantage of a fast heat transfer with a quick start-stop, which is an advantage for applications aiming at storing excess energy from renewable sources[2].

Another potential advantage of magnetic heating is the subject of a controversy, which started in the field of magnetic hyperthermia. In 2002, it was proposed that allowing MNPs to enter *inside* tumor cells could be more efficient because the heat generation as well as the temperature rise, being intracellular, would be more efficient[5]. A few years later, it was convincingly argued, using standard heat diffusion equations, that the temperature gradient around magnetically heated single MNPs or micron-size assemblies of MNPs should not exceed the mK. It means that, at the cell level, the temperature has to be considered as homogeneous[6]. However, in 2010, Villanueva *et al*. showed for the first time that, during *in vitro* experiments, tumor cells could be killed without any global rise of the temperature, renewing

the hypothesis that localized heating occurred and could be efficient to induce cell death[7]. These biology results have since then been confirmed by several groups, including us[8, 9, 10, 11, 12, 13, 14].

Most probes used during standard experiments measure temperatures at the millimeter scale, much larger than the scale where the local thermal gradients are hypothesized to occur. Several groups have developed ingenious strategies to map temperature gradients in the vicinity of the MNP surfaces using molecular[15, 16, 17, 18, 19] or fluorescent[20, 21, 22, 24, 25] probes. All of them led to the conclusion that, indeed, NPs in liquid media produce and sustain a significant temperature gradient (ΔT = [6°C-90°C]) in their immediate vicinity when heated by radiofrequency magnetic fields. In a recent review, Cazares-Cortes[26] summarizes in a figure the results issued from the aforementioned experiments and interprets the general trend as showing a strong thermal gradient from the surface of the nanoparticles to the surrounding medium.

On the theoretical side, things are less unanimous. A comparison with theoretical heat transfer mechanisms would suggest that, with dimension similar to that of the phonons' mean free path, heat transport around MNPs is not diffusive but ballistic, and Fourier law is not valid anymore[15, 27]. On the other side, Keblinski *et al.* suggest that the heat flow in liquids can be well described by the diffusive heat equations even at the nanoscale[6]. Adding to the confusion, some authors give theoretical arguments against nanoscale thermal phenomena [5, 28]. A recent paper from Chiu-Lam and al.[29] summarizes the clash between theoretical predictions and experimental observations. Current investigations on nanoscale thermal transport rather focus on NP-fluid interfacial properties[30, 31, 32].

The convincing experimental results coming from the biology side have led our group – which also works on the catalysis side –, to hope that, in chemical reactions where MNPs are both the heating agents and the catalysts, strong nanoscale gradients could also be observed in the vicinity of MNPs. In applications where energy efficiency matters, such as the Sabatier reaction used for power-to-gas, this would permit to heat the catalyst without heating the support and the reactor, permitting energy savings, a potentiality that we have named "cold catalysis" [33].

In the present article, we report on the measurements, in solid-state samples where MNPs are grafted on a support, of the gradient occurring between the MNPs and their surroundings. To probe the MNP temperature, we have used an original approach, which consists in deducing the MNP temperature from the temperature dependence of their lattice parameter, using X-Ray diffraction (XRD) on a synchrotron beamline. This approach permits, for the first time, to measure the internal temperature of magnetically heated MNPs, and not the temperature in their vicinity. To measure the mean temperature of the medium, a reference material (i.e. with a strong temperature dependence of its lattice parameter) was added to the sample under the form of micron-size boron nitride (BN) particles, the temperature of which was also deduced using the same method. We did not detect any temperature gradient between the MNPs and the medium; if the latter exists, it is within the error bar of our method,

which is estimated to be around 5°C. The potential reasons for this absence of temperature gradient are discussed.

2. Methods

2.1. Magnetic field source

The electromagnet was a toroidal ferrite (Ferroxcube 3C95) winded with Litz wire (RUPALIT Safety V155 480x0.071) and encapsuled in a plastic jacket. The gap has to be as small as possible to enhance the field, but required to be at least 3 mm wide to fit a 2 mm diameter capillary and to avoid to cut the diffracted beam. The gap was opened with a diamond wheel saw and beveled at 38° to permit to get the largest possible portion of the diffracted beam. The electromagnet was mounted in series with a rotary variable air capacitor that is able to support high alternating currents without heating, contrary to chemical capacitors. At maximum power, the setup was fed with a voltage V_{rms}= 56.6 V and an alternating current I_{rms} = 2.5 A (high-speed bipolar amplifier HSA 4052) at frequency f = 270 kHz, for a total power of 140 W. The magnetic field generated in the gap had a maximal intensity $\mu_0 H_{max}$ = 45 mT. The electromagnet was cooled down by a forced air flow through the tubular arm structure.

2.2. Beamline detection

The detector usually used for XRPD, a CMOS 2D detector, was perturbed by the electromagnetic field of the electromagnet. It was replaced by an image plate detector MAR 345. However, the reference diffractogram for the SiRAlOx powder (see below) was measured using the first detector.

3. Results and discussion

The initial studied samples were SiRAlOx-supported (γ-Al_2O_3) catalyst consisting of 10 wt% BN and 13 wt% FeC MNPs that corresponds to 1% volume fraction. As will be explained below, the final samples on which nanoscale temperature measurements have been performed are samples where the NPs have been oxidized. NP synthesis is detailed in the Supplementary Information. TEM structural analysis shows that the NPs are well dispersed with a size distribution of 14.6 $\pm$ 1.1 nm. The measured SAR value in a toluene solution was of ca. 2000 W·g^{-1} under 47 mT magnetic field and 100 kHz frequency. For a typical sample prepared in the glove box, FeC NPs (60 mg, Fe content ca. 75%) were dispersed in toluene (10 ml). Then, the catalyst (SiRAlOx, 400 mg) was added to the dispersion and the mixture sonicated for 20 min. At the end, the excess of toluene was removed under vacuum. The yield is ca. 420 mg of FeC / SiRAlOx and the Fe content determined by Inductively Coupled Plasma (ICP) is 9.15 wt%.

In situ X-Ray powder diffraction (XRPD) measurements were performed at the BM31 line of the Swiss-Norwegian Beamlines located at the European Synchrotron Radiation Facility (ESRF) in Grenoble, France. A scheme of the experimental configuration under magnetic field can be seen in Figure 1. Special attention was given to the geometry of the coil to fit the beamline configuration as well as the field intensity requirements. High-resolution-XRPD data were collected with the standard BM31 setup, using wavelengths of λ = 0.49417 Å. Powder samples were put inside a quartz capillary which had a length of 60 mm, a diameter of 2 mm and a wall

thickness superior to 0.02 mm[34]. Capillaries with 1 mm outer diameter were also used, but the volume of powder was not sufficient to observe a sufficient heating under rf field excitation. The catalyst was diluted with the required amount of hexagonal boron nitride (h-BN) (BNhcp Alfa Aesar 99.5% CAS: 10043- 11- 5), loaded into the quartz capillary and sealed with a high temperature epoxy glue. The sample was heated by a vertical hot air blower for calibration experiments or by the electromagnet.

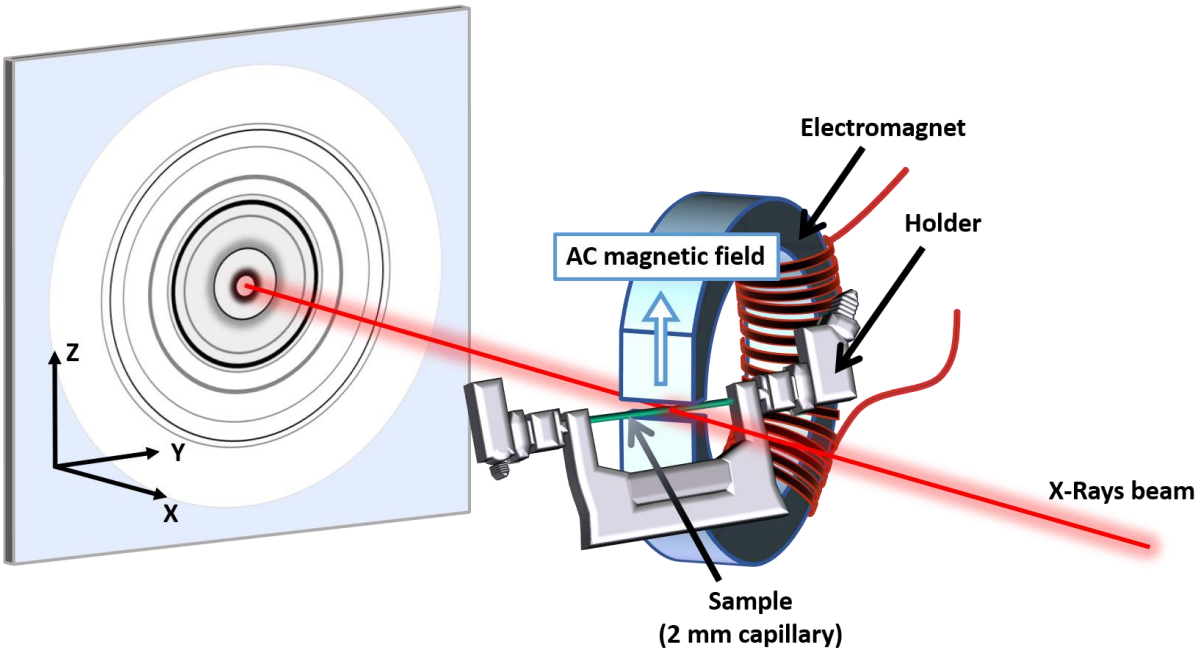

Figure 1. Representation of the X-rays set-up configuration with alternating magnetic field excitation.

The sample was originally designed to make on the same sample the experiments described in this article as well as an in-situ monitoring by XRD and EXAFS of the Sabatier reaction under a high-frequency magnetic field. This explains the structure of our sample, which is composed of FeC MNPs as heating agent supported on SiRAlOx powder.

Figure 2 shows the XRD diffraction of our sample. The SiRAlOx diffractogram shows that the powder is almost amorphous (cf. black curve on Figure 2) and is responsible of the heavy background. The diffraction patterns of the sample show the contributions of the FeC and h-BN phases, broaden by the SiRAlOx background. As a preliminary test to confirm the heating power of the NPs, the sample was heated by the magnetic field in absence of a gas flow. The temperature of the capillary surface, measured by an infrared camera, was 121 °C. Then, we measured the evolution of the sample heated by the hot air blower during an overnight temperature cycle. The sample was heated up to 225°C (blower temperature) before cooling down back to room temperature. The diffraction patterns obtained after heating clearly show an oxidation (green curve on Figure 2) with a phase transformation of the FeC to magnetite (Fe_3O_4) or maghemite (γ-Fe_2O_3). The oxidation was not expected and we

guess it is due to a leak from the capillary's seal. The fit made with the software Maud[35] highlights the different phases of the species present inside the sample. The presence of the Fe_3O_4 phase is consistent with the standard pattern for JCPDS Card No. (79 - 0417) Magnetite

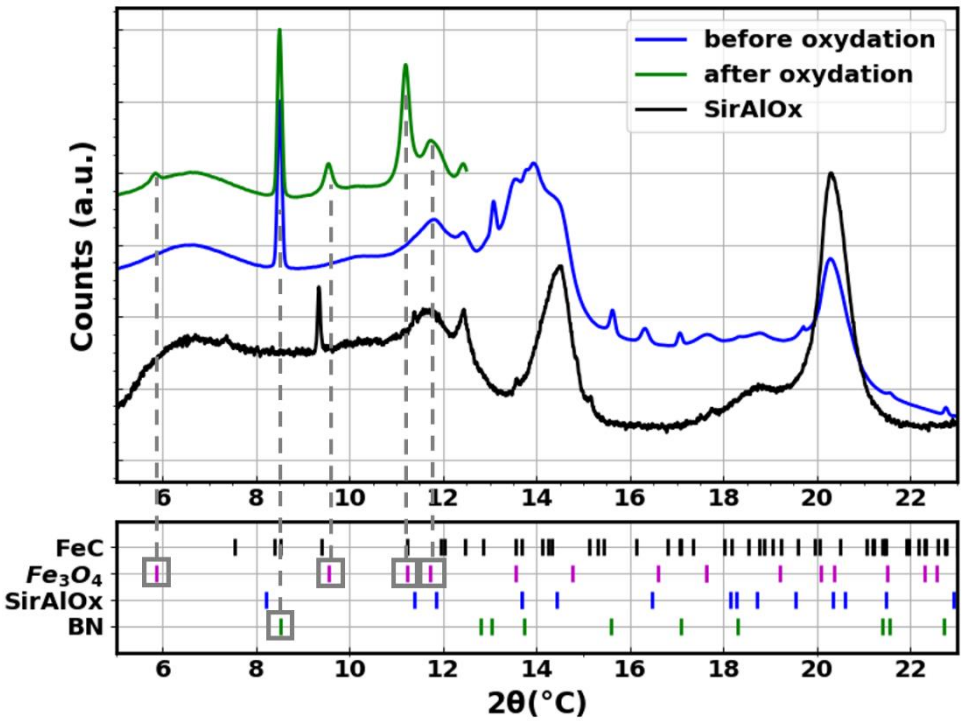

Figure 2. Diffractogram of SiRAlOx support (black curve), FeC supported sample before (blue curve) and after (green curve) heating. The positions of the different phases of FeC, Fe_3O_4, SiRAlOx and h-BN determined by the fit are indicated on the bottom panel. Vertical dotted lines are guide for the eyes to see the Fe_3O_4 phases corresponding to peaks in the oxidized sample.

– synthetic[36] and permit to completely fit the diffractogram, suggesting that the FeC was fully oxidized and disappeared below the detection level inside the background. The SiRAlOx alone was fitted with Maud and included as a background baseline. The fit was performed using only the Fd-3m:1 cubic phase for the Fe_3O_4 and the P-6 hexagonal phase for the BN. We reasonably assumed that no further evolution subsists at the issue of the oxidation that could affect the lattice parameter and impair the results. The peak resolution is strongly degraded by the SiRAlOx background and we can only base the analysis of the diffraction angle shift in temperature on high intensity peaks. Hence, we focus on the small angles part of the diffractogram, namely the range $2\theta = [4°, 12.5°]$, where different Fe_3O_4 planes, in addition to h-BN peak, are clearly identifiable after oxidation (the positions of the peak of interest are indicated by grey vertical dotted lines on Figure 2).

The evolution of the diffraction pattern in the temperature range T = [23°C - 190°C] is presented in Figure 3. A zoom in on each peak helps the visibility. There are four Fe_3O_4 peaks corresponding to the [111], [220], [311] and [222] crystallographic planes centered at 5.85°, 8.5°, 9.55°, 11.2° and 11.8° respectively. The Fe_3O_4 [222] plane is merged with a SiRAlOx [110] plane. The peak centered at 8.52° corresponds to the h-BN [002] plane. Clearly the shift of the

boron nitride peak in temperature is more important than for the other peaks. It will be used as a reference to know the mean temperature inside the sample.

In a material the lattice parameter *a* is given by Bragg's law:

$$a = \frac{n\lambda}{2}\frac{\sqrt{h^2 + k^2 + l^2}}{\sin\theta}\ , \qquad (1)$$

with *h*, *k*, *l* the Miller's indices characterizing a plane, λ the X-ray wavelength and θ the diffraction angle. The lattice parameter variation is related to the temperature variation $\Delta T = T - T_0$ by the thermal expansion coefficient α_c ($\sim 10^{-5} K^{-1}$ in our case):

$$a = a_0(1 + \alpha_c \Delta T)\ , \qquad (2)$$

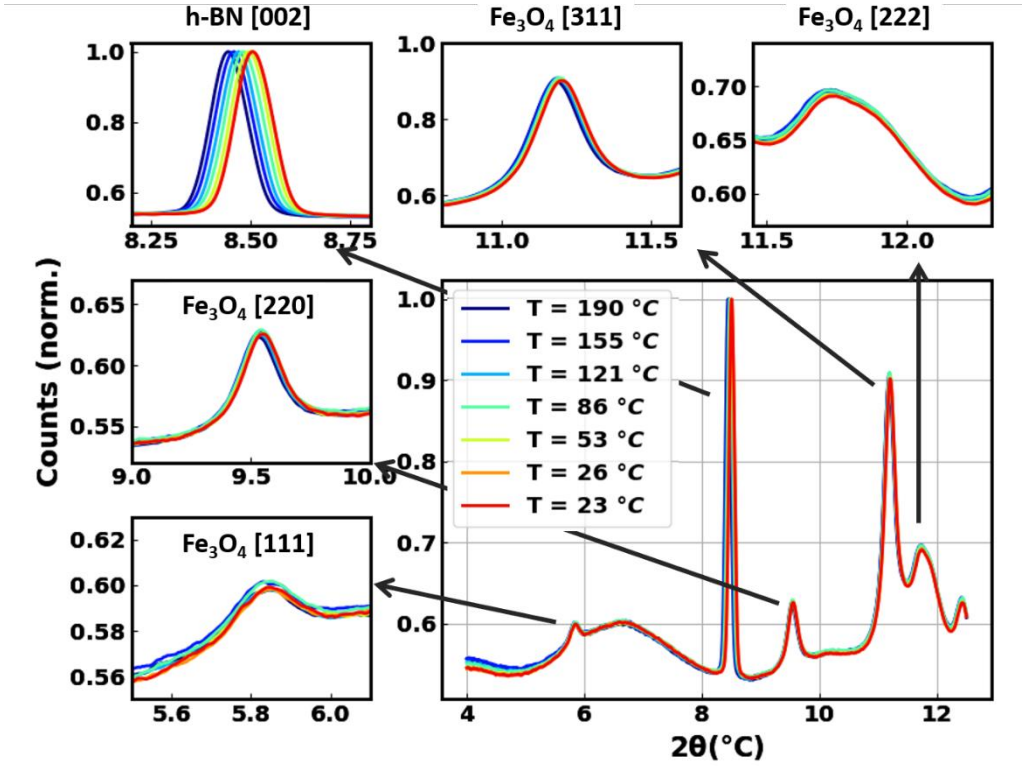

Figure 3. Evolution of Fe_3O_4 [111], [220], [311], [222] and BN [002] planes in function of the temperature.

The calibration law $\Delta(2\theta) = 2\theta_T - 2\theta_{T_0} = f(\Delta T)$ of each plane is presented in Figure 4. The 2θ position of each peak is determined from a fit with a gaussian function and is related to the lattice parameter via equation (1). The error bars on the heating ΔT are obtained from the covariance matrix of the least squares gaussian fit function. The standard deviation on the temperature, related to the measurement error using the blower, was arbitrarily fixed to an overestimated value of 1°C. The lattice parameter is calculated by an orthogonal distance regression fit of equation (2) that includes the standard deviation (error bars). The R-square parameter corresponding to the variance of the data with a linear regression fit is given in the legend. An agreement better than 1% is obtained for the h-BN [002] and Fe_3O_4 [311] planes. It corresponds to a thermal expansion coefficient of the c-axis $\alpha_c = 44\ 10^{-6}\ K^{-1}$ and a-axis

$\alpha_a = 10.94\ 10^{-6}\ K^{-1}$ respectively which are in good agreement with the literature (cf. Table 1). We will focus on these two peaks to probe the temperature variation under magnetic field with the best accuracy.

	h-BN [002]		Fe_3O_4 [311]	
	Experiment	**Literature** [37]	**Experiment**	**Literature** [38]
a, $c_{25°C}$	c = 6.6626 Å	c = 6.66 Å	a = 8.3991 Å	a = 8.397 Å
α_c	$44x10^{-6}\ K^{-1}$	$37x10^{-6}\ K^{-1}$	$10.94x10^{-6}\ K^{-1}$	$9{,}5x10^{-6}\ K^{-1}$

Table 1. Lattice parameter and thermal expansion coefficient of BN [002] and Fe_3O_4 [311] planes calculated from the linear fit of the data shown in Figure 4 and comparison with the literature.

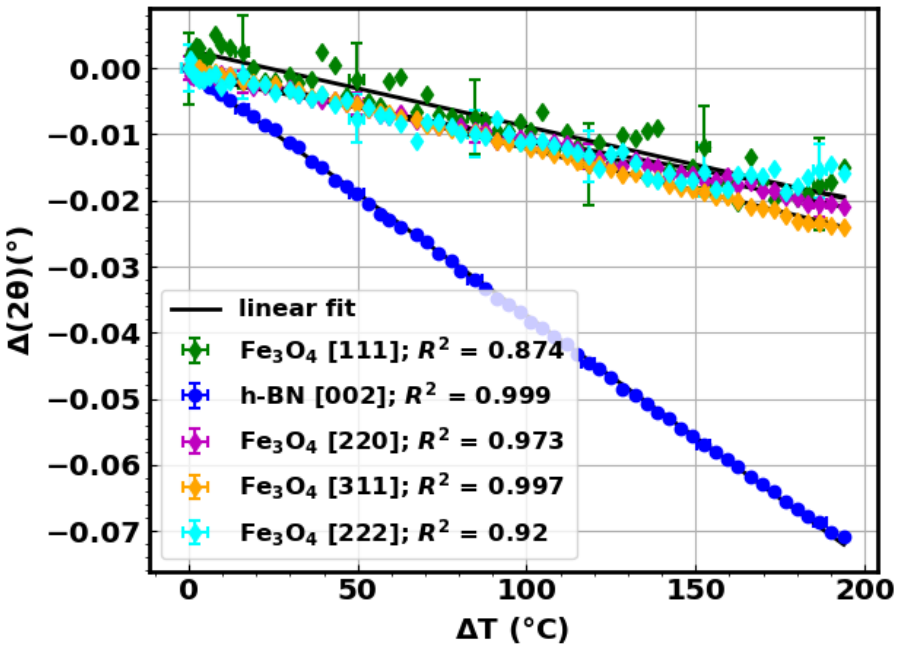

Figure 4. Calibration curve of the lattice parameter shift in function of the temperature.

The hot air blower was replaced by the electromagnet for experiments described thereafter. X-rays diffraction pattern was recorded at regular interval of time before turning on the electromagnet (room temperature regime), under magnetic field application (heating regime) and after the field was turned off (cooling temperature regime). Due to the time scales of the measuring technique, only stationary temperature gradients could be measured. The possibility to measure transient temperature gradient profile and how it may change the result of the experiment will be discussed at the end of the article. The angle shift of the different peaks was measured and converted into a temperature value using the calibration law previously obtained. The heating of the BN and Fe_3O_4 NPs is shown in Figure 5. They are at the same temperature (no heating) before applying the magnetic field. Then, the field is turned on and the particles heating evolves similarly. Finally, when the field is turned off, the temperature inside the NPs decreases at the same speed.

Using the initial slope method, the temperature sweeping rate permits to estimate a lower limit for the SAR of the particles: 0.5 W/g. One reason for this low value is that particles are supported on a solid matrix and thus not able to form chains[39]. Part of the heat is also afforded to the sample from the electromagnet. It affects h-BN and iron peaks, similarly, acting as an offset in the measurements. The heating measured by the IR camera at t = 1142 sec (Figure 5) is ΔT = 95 °C on the surface of the capillary and ΔT = 6 °C on the surface of the electromagnet. The thermal inertia of the electromagnet (with a maximal heating of ΔT = 49 °C) is responsible for the residual heating observed after the magnetic field was turned off".

We measure a maximum heating for the MNPs of $\Delta T = 63.7 \pm 4.6°C$ and for the h-BN particles of $\Delta T = 62.7 \pm 0.3°C$. The maximum heating ΔT obtained from the other peaks corresponding to different Fe_3O_4 crystallographic planes is similar even though the measurement uncertainty is more important (cf. Table 2) due to a poorer resolution. These results show that there is no significant temperature gradient between the Fe_3O_4 MNP core and the surrounding powder.

	h-BN [002]	Fe_3O_4 [311]	Fe_3O_4 [220]	Fe_3O_4 [222]	Fe_3O_4 [111]
ΔT	**62.70**	**63.68**	57.52	60.59	114.18
σ	**0.35**	**4.62**	19.36	37.98	76.56

Table 2. Maximum heating and standard deviation calculated from the BN and Fe_3O_4 peak shifts under RF magnetic field.

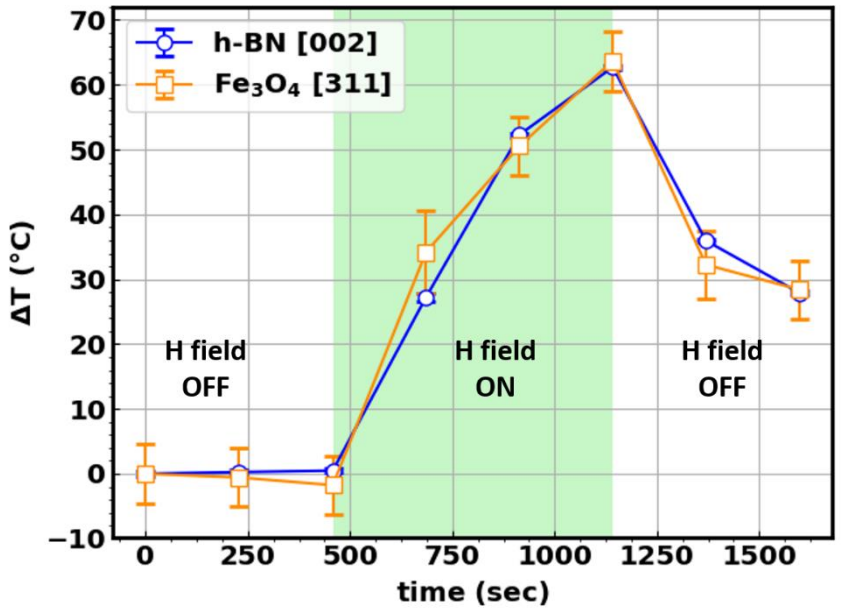

Figure 5. Heating inside the FeC MNPs and BN NPs in presence (H field ON area) and absence (H field OFF area) of a RF magnetic field. The temperature variation is calculated from the lattice parameter variation of Fe_3O_4 [311] and BN [002] planes respectively.

At first sight, this result could appear in contradiction with experimental results of the literature [15, 17, 18, 19, 21, 23]. However, two important differences between previous experimental results and ours should be noted, and might be at the origin of the difference: i) all other

groups evaluated the temperature using the physical properties of an organic agent external to the MNPs: the thermal degradation of a ligand[15, 17, 18, 19] or the fluorescence of a lanthanide complex[21, 23]. ii) all other groups performed their experiments on colloidal solutions, i.e. with MNPs in liquid phase.

With respect to i), we wonder if it would be possible that the large temperatures measured by organic entities in the vicinity of the magnetically excited MNPs could be due to powerful heat impulses. Indeed, the total heat power delivered by single-domain NPs during one cycle of the field equals the loop area. Nevertheless, the heat power is not delivered continuously along time, but presents strong intensity pulses when magnetization jumps, as illustrated in a typical example in Figure 6. The most extreme case occurs when the magnetic field is aligned with the NP anisotropy axis. In this case, the hysteresis loop is a rectangle so all the energy is concentrated in two intense power peaks occurring at the coercive field of the NP. A hypothesis to consider is that the energy released this way would be high enough to break thermosensitive covalent bonds of ligands or decrease the fluorescence of molecules, for example, whereas it would not if the energy was released continuously (green dotted curve in Figure 6). In this case, experiments would conclude to a local heating even though there is none.

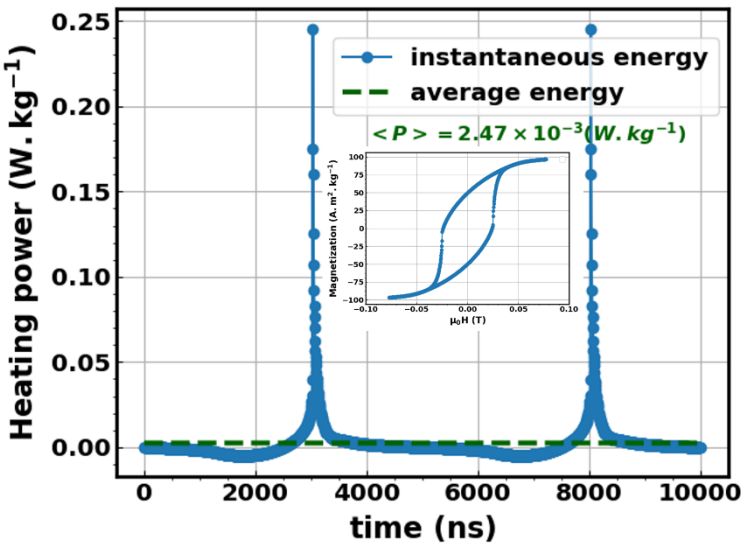

Figure 6 – Instantaneous (blue line) and time averaged (green dotted line) power released by one NP during one hysteresis loop (shown in inset).

With respect to ii), it is a well-known fact that, in liquid phase, MNPs excited by an external magnetic field form chains, which are sometimes several tens or hundreds of microns wide, depending on the MNP properties, their functionalization, the magnetic field amplitude, and so forth[39, 40, 41, 42]. When such chains form, the measured "local" temperature is not the temperature at the surface of an isolated nanoscale object, but the temperature at the surface and/or inside a micron-scale magnetically heated assembly of MNPs. Since the temperature gradient at the surface or inside an object heated from inside scales as the volume/surface ratio of this object, one can easily conclude that the temperature gradient might be much larger in these chains than in isolated MNPs. For instance, our group has recently shown that,

when millimeter chains are formed, gradients which are probably of the order of several tens of degrees build up[42]. Although this hypothesis is appealing and casts doubts on the experimental results obtained by other groups, a detailed reading of these works make, in our opinion, this hypothesis unlikely to explain all, if any, experimental results. In Clerc and al.[20], MNPs are internalized in lysosomes so only assemblies with a maximum size of one micron could form, which is insufficient to generate a 14°C gradient using standard diffusion equations. In the case of Piñol and al.[23], the fact that small (10 nm) superparamagnetic particles are embedded in a rather thick polymer matrix makes unlikely the appearance of strong dipolar interactions between beads and thus the formation of thick chains. In Riedinger et al., particles are 15 nm in diameter, a size where significant dipolar interactions could build up, but significant temperature gradients are observed even when a small magnetic field of 9 mT is applied[15].

A last hypothesis related to ii) is that, in our case, heat diffusion through the solid support would be much more efficient than in a liquid environment. However, to explain the discrepancy between our results and the ones from the literature, the difference in the diffusion coefficient should have to be of several orders of magnitude, as already discussed in several previous experimental results[15, 23]. Experiments similar to the ones described here but performed on particles in liquid could permit to eliminate or reinforce the hypotheses formulated above. For now, the problem remains open to new experimental and theoretical investigations.

4. **Conclusions**

We have measured the inner temperature of MNPs heated by a rf magnetic field. It is a turnabout in the methodology compare to all previous experiments that consist in designing probes that get closer to the surface of the nanoparticle. Our method is a powerful tool to measure the gradient between the internal temperature of the MNPs and the mean temperature of the sample. It could be used to measure the temperature gradient of particles supported on different media, or into water, since the gradient could strongly vary depending on the nature of the MNP-substrate link. Our results show that, if a gradient appears at the interface between the MNPs and the solid-state catalytic bed, it is of rather small amplitude. Our work thus brings a new brick on the active debate on the nanoscale gradient of magnetically heated MNPs.

Conflict of Interest: The authors declare no competing financial interest.

Supporting Information Available: Detailed synthesis of the nanoparticles.

Acknowledgements: The authors thank ERC Advanced Grant (MONACAT 2015-694159) for financial support. The personnel of the Swiss-Norwegian Beamlines are acknowledged for experimental assistance (experiment MA-4029BM31@SNBL).

References

[1] Ortgies, D.H. ; Teran, F.J.; Rocha, U.; de la Cueva, L.; Salas, G.; Cabrera, D.; Vanetsev, A.S.; Rähn, M.; Sammelselg, V.; Orlovskii, Y.V.; and al. ; Optomagnetic Nanoplatforms for In Situ Controlled Hyperthermia. *Adv. Funct. Mater.* **2018**, *28*, 1704434-1704444. https://doi.org/10.1002/adfm.201704434.

[2] Bordet, A. ; Lacroix, L.-M.; Fazzini, P.-F.; Carrey, J.; Soulantica, K.; Chaudret, B. ; *Magnetically Induced Continuous CO2 Hydrogenation Using Composite Iron Carbide Nanoparticles of Exceptionally High Heating Power, Angew. Chem., Int. Ed.* **2016**, *55*, 15894-15898. https://doi.org/10.1002/anie.201609477.

[3] Niether, C. ; Faure, S.; Bordet, A.; Deseure, J.; Chatenet, M.; Carrey, J.; Chaudret, B. ; Improved Water Electrolysis Using Magnetic Heating of FeC–Ni Core–Shell Nanoparticles, *Nat. Energy **2018**, 3*, 476-483. https://doi.org/10.1038/s41560-018-0132-1.

[4] Lacroix, L.-M.; Lachaize, S.; Falqui, A.; Respaud, M.; Chaudret, B.; *Iron Nanoparticle Growth in Organic Superstructures, J. Am. Chem. Soc.* **2009**, *131*, 549-557. https://doi.org/10.1021/ja805719c.

[5] Rabin, Y.; Is Intracellular Hyperthermia Superior to Extracellular Hyperthermia in the Thermal Sense?", *Int. J. Hyperthermia* **2002**, *18*, 194-202. https://doi.org/10.1080/02656730110116713.

[6] Keblinski, P.; Cahill, D.G.; Bodapati, A.; Sullivan, C.R.; Taton, T.A.; Limits of Localized Heating by Electromagnetically Excited Nanoparticles, J. Appl. Phys. **2006**, *100*, 054305-054309. https://doi.org/10.1063/1.2335783.

[7] Villanueva, A.; de la Presa, P.; Alonso, J.M.; Rueda, T.; Martínez, A.; Crespo, P.; Morales, M.P.; Gonzalez-Fernandez, M.A.; Valdés, J.; Rivero, G.; Hyperthermia HeLa Cell Treatment with Silica-Coated Manganese Oxide Nanoparticles, *J. Phys. Chem. C*, **2010**, *114*, 1976-1981. https://doi.org/10.1021/jp907046f.

[8] Hamad-Schifferli, K.; Schwartz, J. J.; Santos, A. T.; Zhang, S.; Jacobson, J. M.; Remote Electronic Control of DNA Hybridization through Inductive Coupling to an Attached Metal Nanocrystal Antenna, Nature **2002**, 415, 152–155. https://doi.org/10.1038/415152a.

[9] Creixell, M.; Bohorquez, A.C.; Torres-Lugo, M.; Rinaldi, C.; EGFR-Targeted Magnetic Nanoparticle Heaters Kill Cancer Cells without a Perceptible Temperature Rise, ACS Nano **2011**, *5*, 7124-7129. https://doi.org/10.1021/nn201822b.

[10] Sanchez, C.; El Hajj Diab, D. ; Connord, V.; Clerc, P.; Meunier, E.; Pipy, B.; Payré, B.; Carrey, J.; Gigoux V.; Fourmy, D. ; Targeting a G-protein Coupled Receptor Overexpressed in Endocrine Tumors by Magnetic Nanoparticles to Induce Cell Death. ACS Nano **2014**, *8*, 1350-1363. https://doi.org/10.1021/nn404954s.

[11] Bastus, N. G.; Kogan, M. J.; Amigo, R.; Grillo-Bosch, D.; Araya, E.; Turiel, A.; Labarta, A.; Giralt, E.; Puntes, V. F. ; Gold Nanoparticles for Selective and Remote Heating of β-amyloid Protein Aggregates. Mater. Sci. Eng. **2007**, *27*, 1236-1240. https://doi.org/10.1016/j.msec.2006.08.003.

[12] Xu, Y.; Mahmood, M.; Li, Z.; Dervishi, E. Trigwell, S.; Zharov, V. P.; Ali, N.; Saini, V.; Biris, A. R.; Lupu, D.; and al. ; Cobalt Nanoparticles Coated with Graphitic Shells as Localized Radio Frequency Absorbers for Cancer Therapy. Nanotechnology **2008**, *19*, 435102-435111. https://doi.org/10.1088/0957-4484/19/43/435102.

[13] del Rosal, B.; Carrasco, E.; Ren, F.; Benayas, A.; Vetrone, F. Sanz-Rodríguez, F.; Ma, D.; Juarranz, A.; Jaque, D. ; Infrared-Emitting QDs for Thermal Therapy with Real-Time Subcutaneous Temperature Feedback, Adv. Funct. Mater. **2016**, *26*, 6060-6068. https://doi.org/10.1002/adfm.201601953.

[14] Huang, H.; Delikanli, S.; Zeng, H.; Ferkey, D. M.; Pralle, A.; Remote Control of Ion Channels and Neurons Through Magnetic-Field Heating of Nanoparticles. Nat. Nanotechnol. **2010**, *5*, 602–606. https://doi.org/10.1038/nnano.2010.125.

[15] Riedinger, A.; Guardia, P.; Curcio, A.; Garcia, M. A.; Cingolani, R.; Manna, L.; Pellegrino, T.; Subnanometer Local Temperature Probing and Remotely Controlled Drug Release Based on Azo-Functionalized Iron Oxide Nanoparticles. Nano Lett. **2013**, *13*, 2399−2406. https://doi.org/10.1021/nl400188q.

[16] Lee, J.; Govorov, A.O.; Kotov, N.A.; Nanoparticle Assemblies with Molecular Springs: A Nanoscale Thermometer. Angew. Chem. **2005**, *44*, 7439-7442. https://doi.org/10.1002/anie.200501264.

[17] Dias, J.T.; Moros, M.; del Pino, P.; Rivera, S.; Grazú, V.; de la Fuente, J.M.; DNA as a Molecular Local Thermal Probe for the Analysis of Magnetic Hyperthermia. Angew. Chem. Int. **2013**, *52***,** 11526-11529. https://doi.org/10.1002/anie.201305835.

[18] N'Guyen, T.T.T. ; Duong, H.T.T. ; Basuki, J.; Montembault, V.; Pascual, S.; Guibert, C.; Fresnais, J.; Boyer, C.; Whittaker, M.R.; Davis, T.P.; and al. ; Functional Iron Oxide Magnetic Nanoparticles with Hyperthermia-Induced Drug Release Ability by Using a Combination of Orthogonal Click Reactions. Angew. Chem. Int. **2013,** *52*, 14152-14156. https://doi.org/10.1002/anie.201306724.

[19] Griffete, N.; Fresnais, J.; Espinosa, A.; Wilhelm, C.; Bee, A.; Menager, C. ; Design of Magnetic Molecularly Imprinted Polymer Nanoparticles for Controlled Release of Doxorubicin under an Alternating Magnetic Field in Athermal Conditions. *Nanoscale*, **2015**, *7*, 18891-18896. https://doi.org/10.1039/C5NR06133D.

[20] Clerc, P.; Jeanjean, P.; Halalli, N.; Gougeon, M.; Pipy, B.; Carrey, J.; Fourmy, D.; Gigoux, V. ; Targeted Magnetic Intra-lysosomal Hyperthermia Produces Lysosomal Reactive Oxygen Species and Causes Caspase-1 Dependent Cell Death", J. Control Release **2018**, *270*, 120-134. https://doi.org/10.1016/j.jconrel.2017.11.050.

[21] Dong J.; Zink, J. I.; Taking the Temperature of the Interiors of Magnetically Heated Nanoparticles. ACS Nano **2014**, *8*, 5199-5207. https://dx.doi.org/10.1021%2Fnn501250e.

[22] Brites, C.D.S.; Lima, P.P.; Silva, N.J.O.; Millán, A.; Amaral, V.S.; Palacio, F.; Carlos, L.D.; A Luminescent Molecular Thermometer for Long-Term Absolute Temperature Measurements at the Nanoscale. Adv. Mater. **2010**, *22*, 4499-4504. https://doi.org/10.1002/adma.201001780.

[23] Piñol, R.; Brites, C. D. S.; Bustamante, R.; Martínez, A.; Silva, N. J. O.; Murillo, J. L.; Cases, R.; Carrey, J.; Estepa, C.; Sosa, C.; and al.; Joining Time-Resolved Thermometry and Magnetic-Induced Heating in a Single Nanoparticle Unveils Intriguing Thermal Properties", ACS Nano **2015**, *9*, 3134-3142. https://doi.org/10.1021/acsnano.5b00059.

[24] Polo-Corrales, L.; Rinaldi, C.; Monitoring Iron Oxide Nanoparticle Surface Temperature in an Alternating Magnetic Field Using Thermo Responsive Fluorescent Polymers. J. Appl. Phys. **2012**, *111*, 07B334. https://doi.org/10.1063/1.3680532.

[25] Gupta, A.; Kane, R.S.; Borca-Tasciuc, D.A.; Local Temperature Measurement in the Vicinity of Electromagnetically Heated Magnetite and Gold Nanoparticles. J. Appl. Phys. **2010**, *108*, 064901-064908. https://doi.org/10.1063/1.3485601.

[26] Cazares-Cortes, E.; Cabana, S.; Boitard, C.; Nehlig, E.; Griffete, N.; Fresnais, J.; Wilhelm, C.; Abou-Hassan, A.; Ménager, C. ; Recent Insights in Magnetic Hyperthermia: From the "Hot-Spot" Effect for Local Delivery to Combined Magneto-Photo-Thermia Using Magnetoplasmonic Hybrids", Adv. Drug Deliv.Rev. **2019**, *138*, 233-246. https://doi.org/10.1016/j.addr.2018.10.016.

[27] Chen, G.; Nonlocal and Nonequilibrium Heat Conduction in the Vicinity of Nanoparticles. J. Heat Transfer **1996**, *118*, 539-545. https://doi.org/10.1115/1.2822665.

[28] Kozissnik, B.; Bohorquez, A. C.; Dobson, J.; Rinaldi, C.; Magnetic Fluid Hyperthermia: Advances, Challenges, and Opportunity. *Int. J. Hyperthermia* **2013**, *29*, 706-714. https://doi.org/10.3109/02656736.2013.837200.

[29] Chiu-Lam, A.; Rinaldi. C.; Nanoscale Thermal Phenomena in the Vicinity of Magnetic Nanoparticles in Alternating Magnetic Fields. Adv. Funct. *Mater*. **2016**, *22*, 3933-3941. https://dx.doi.org/10.1002%2Fadfm.201505256.

[30] Cahill, D. G.; Braun, P. V.; Chen, G.; Clarke, D. R.; Fan, S.; Goodson, K. E.; Keblinski, P.; King, W. P.; Mahan, G. D.; Majumdar, A.; Maris, H. J.; Phillpot, S. R.; Pop, E.; Shi, L; and al.; Nanoscale Thermal Transport. II. 2003–2012. Appl. Phys. Rev. **2014**, *1*, 011305-011350. https://doi.org/10.1063/1.4832615.

[31] Chiavazzo, E.; Fasano, M.; Asinari P.; Decuzzi, P. ; Scaling Behaviour for the Water Transport in Nanoconfined Geometries. Nat. Commun., **2014**, *5*, 3565-3575. https://doi.org/10.1038/ncomms4565.

[32] Shenogina, N.; Godawat, R. Keblinski P.; Garde, S. ; How Wetting and Adhesion Affect Thermal Conductance of a Range of Hydrophobic to Hydrophilic Aqueous Interfaces. Phys. Rev. Lett., **2009**, *102*, 156101-156104. https://ui.adsabs.harvard.edu/link_gateway/2009PhRvL.102o6101S/doi:10.1103/PhysRevLett.102.156101.

[33] Meffre, A. Mehdaoui, B.; Connord, V.; Carrey, J.; Francesco Fazzini, P.; Lachaize, S.; Respaud, M.; Chaudret, B.; Complex Nano-objects Displaying Both Magnetic and Catalytic Properties: A Proof of Concept for Magnetically Induced Heterogeneous Catalysis. Nano Lett. **2015**, *15*, 3241-3248. https://doi.org/10.1021/acs.nanolett.5b00446.

[34] Tsakoumis, N. E.; Voronov, A.; Ronning, M.; van Beek, W.; Borg, O.; Rytter E.; Holmen, A. ; Fischer–Tropsch Synthesis: An XAS/XRPD Combined *In Situ* Study from Catalyst Activation to Deactivation. *J. Catal.*, **2012**, *291*, 138-148. https://doi.org/10.1016/j.jcat.2012.04.018.

[35] Lutterotti, L.; Campostrini, R.; Gialanella, S.; Di Maggio, R.; Microstructural Characterisation of Amorphous and Nanocrystalline Structures Through Diffraction Methods. JMNM **2000**, *8*, 657–664. https://doi.org/10.4028/www.scientific.net/JMNM.8.657.

[36] El Ghandoor, H.; Zidan, H.; Khalil, M.; Ismail, M.I.M.; Synthesis and Some Physical Properties of Magnetite (Fe3O4) Nanoparticles. *Int. J. Electrochem. Sci.,* **2012**, *7***,** 5734-5745. http://www.electrochemsci.org/papers/vol7/7065734.pdf

[37] Hamdi I.; Meskini, N.; Ab Initio Study of the Structural, Elastic, Vibrational and Thermodynamic Properties of the Hexagonal Boron Nitride: Performance of LDA and GGA. Physica B, **2010**, *405*, 2785 - 2794. https://doi.org/10.1016/j.physb.2010.03.070.

[38] Touloukian Y.S.; Kirby, R.K.; Thermophysical Properties of Matter **1977,** *13*, 247-250.

[39] Serantes, D.; Baldomir, D.; Martinez-Boubeta, C.; Simeonidis, K.; Angelakeris, M.; Natividad, E.; Castro, M.; Mediano, A.; Chen, D.-X.; Sanchez, A.; and al.; Influence of Dipolar Interactions on Hyperthermia Properties of Ferromagnetic Particles. J. Appl. Phys. **2010**, *108*, 073918-073923. https://doi.org/10.1063/1.3488881.

[40] Mehdaoui, B.; Meffre, A.; Carrey, J.; Lachaize, S.; Lacroix, L.M.; Gougeon, M.; Chaudret, B.; Respaud, M.; Increase of Magnetic Hyperthermia Efficiency Due to Dipolar Interactions in Low-Anisotropy Magnetic Nanoparticles: Theoretical and Experimental Results. Adv. Funct. Mater., **2011**, 21, 4573-4582.

https://arxiv.org/ct?url=https%3A%2F%2Fdx.doi.org%2F10.1103%2FPhysRevB.87.174419&v=d94ac45a.

[41] Saville, S.L.; Qi, B. ; Baker, J.; Stone, R.; Camley, R.E.; Livesey, K.L.; Ye, L.; Crawford, T.M.; Thompson; Mefford, O.; The Effect of Magnetically Induced Linear Aggregates on Proton Transverse Relaxation Rates of Aqueous Suspensions of Polymer Coated Magnetic Nanoparticles. J. Colloid Interface Sci., **2014**, *424*, 2152-2163. https://doi.org/10.1039/C3NR32979H.

[42] Asensio, J.M. ; Marbaix, J.; Mille, N.; Lacroix, L.-M.; Soulantica, K.; Fazzini, P.-F.; Carrey, J.; Chaudret, B.; *To Heat or not to Heat: a Study of the Performances of Iron Carbide Nanoparticles in Magnetic Heating. Nanoscale* **2019**, *11*, 5402-5411. https://doi.org/10.1039/C8NR10235J.

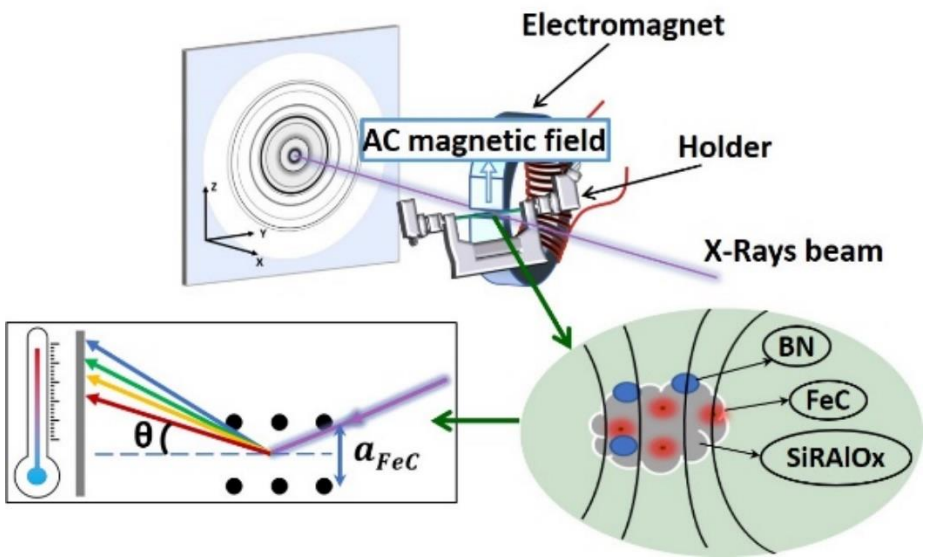

Figure 7. TOC Graphic